International Journal of Hydrogen Energy 111 (2025) 681–695

Contents lists available at ScienceDirect

International Journal of Hydrogen Energy

journal homepage: www.elsevier.com/locate/he

Understanding the mechanism of hydrogen storage on pristine B_2CO monolayer: A DFT study

Rushba Zulfiqar [a], Abdul Majid [a,*], Mohammad Alkhedher [b], Sajjad Haider [c], Kamran Alam [d], Salahuddin Khan [e]

[a] Department of Physics, University of Gujrat, Gujrat, 50700, Pakistan
[b] Mechanical and Industrial Engineering Department, Abu Dhabi University, Abu Dhabi, 59911, United Arab Emirates
[c] Chemical Engineering Department, College of Engineering, King Saud University, P.O.Box 800, Riyadh, 11421, Saudi Arabia
[d] VITO (Flemish Institute for Technological Research), Separation and Conversion Technology, Boeretang 200, 2400, Mol, Belgium
[e] College of Engineering, King Saud University, P.O.Box 800, Riyadh, 11421, Saudi Arabia

ARTICLE INFO

Handling Editor: Dr A Bhatnagar

Keywords:
B_2CO monolayer
Hydrogen storage
Stability
Physisorption

ABSTRACT

The search of a cost-effective material with high gravimetric capacity and efficient reversibility to store hydrogen is a crucial subject these days. In this work, we systematically investigated the underlying mechanism to store hydrogen on pristine B_2CO monolayer by employing density functional theory (DFT). The results demonstrate that the average adsorption energy for H_2 molecules on the B_2CO monolayer is calculated to be −0.614 eV, with individual adsorption energies ranging from - 0.066 eV to −1.712 eV for successive adsorptions. The electrostatic nature of H_2 interactions with the B_2CO monolayer is confirmed via density of states (DOS) and electron localization function (ELF) analyses. The PDOS analysis shows that hydrogen adsorption on the B_2CO monolayer introduces low-energy states (−4 to −6 eV) without significantly altering the band gap. The material's gravimetric and volumetric hydrogen storage capacities are found to be 5.94 wt% and 103 g/L, respectively. The dehydrogenation temperature evaluated to be 785 K to predict reversibility of material. The desorption temperature calculated via the van 't Hoff model has shown that B_2CO monolayer could operate as reversible hydrogen storage media under practical conditions. The Periodic energy decomposition (PEDA) analysis outcomes proved that H_2 molecules interactions with material are attractive in nature. The simulation plots for the nudged elastic band (NEB) indicate that there is a remarkably low energy barrier observed during the adsorption of hydrogen into the material along the specified paths. The findings of this study suggest that the B_2CO monolayer is potential candidate with effective, reversible, and substantial H_2 storage capacity under realistic conditions.

1. Introduction

There is continues energy demand with each passing day, while conventional fossil fuel reserves remain finite. Additionally, the burning of fossil fuels leads to the discharge of carbon dioxide (CO_2) and assorted pollutants. Hence, the discovery of unconventional energy sources that can eventually substitute fossil fuels is of utmost importance [1,2]. In quest of this progress, hydrogen gas (H_2) predicted to be an ideal candidate as an alternative source of energy storage due to its plentiful and sustainable qualities [3–5]. Beside these assets, hydrogen boasts a high energy density and is completely ecologically friendly, as its combustion byproduct is water (H_2O) [6]. The idea of hydrogen economy which envisions a system where hydrogen is a key component in fulfilling our energy needs, encompassing hydrogen-based transportation, storage, and production methods [4]. It has substantially greater energy density (120 MJ kg^{-1}) compared to any other hydrocarbon, approximately three times the energy density of gasoline (44 MJ kg^{-1}) [7]. Therefore, hydrogen demonstrates its potential as an energy carrier [8]. Nevertheless, there are some strategies that need to be addressed currently to achieve a hydrogen economy, including hydrogen production and storage. Despite these facts and beyond usage in energy storing system, hydrogen serves as a means of supplying energy in a useable form due to its inherent compatibility with fuel cells and superior efficiency, with a rate of 60 % as compare to gasoline's or

* Corresponding author.
E-mail address: abdulmajid40@yahoo.com (A. Majid).

https://doi.org/10.1016/j.ijhydene.2025.02.322
Received 29 September 2024; Received in revised form 20 January 2025; Accepted 19 February 2025
Available online 27 February 2025

diesel's 45 % [9,10]. Although hydrogen is considered to be a clean source of energy, its use is currently constrained by significant challenges related to efficient storage and transportation [11]. There are two conventional methods that have already been used to store hydrogen: as a compressed gas or as a liquefied gas. The traditional methods, however, both come with safety risks and are costly. In the first method, hydrogen energy is compressed and stored in a tank [12] and to address safety concerns, a large vessel equipped with a specially designed carbon-reinforced fiber tank is necessary [13]. The other method, in which cryogenic liquefied hydrogen is stored to avoid high compression, requires very low temperatures from a practical application perspective [14,15]. In addition to these approaches, hydrogen may also be stored in a solid state by three efficient adsorption phenomena. Chemisorption occurs when the H_2 molecule dissociates into two individual atoms and forms chemical bonds with the adsorbent. In quasi-molecular adsorption, the adhesive strength lies midway between physisorption and chemisorption. In the physisorption process, the H_2 molecule remains loosely bound to the surface of the adsorbent [16,17]. The method of physical storage is considered as more efficient because with this way hydrogen becomes more reversible when there is a significant surface-to-volume ratio due to the influence of van der Waals interactions [18]. For physical adsorption, two key factors play a crucial role: the energy required to adsorb H_2 molecules and the surface area-to-volume ratio of the host material, both of which determine the overall efficiency [19,20]. Therefore, efficient hydrogen storage is a critical focus of research, with efforts aimed at identifying materials with high hydrogen adsorption capacity. It has been recommended that practical storage materials should achieve at least 5.5 wt% gravimetric hydrogen density and an average adsorption energy per H_2 molecule between 0.15 and 0.6 eV [4,7,21]. Many materials have been thoroughly researched and proven to be highly effective for storage purposes [22]. These materials include metal hydrides which form through strong interactions between hydrogen molecules and metal matrix [23,24]. However, they have a major concern regarding the reversibility of H_2, as individual hydrogen atoms form strong chemical bonds through the chemisorption process within the host material [25]. The materials of different kinds, e.g. metal alloys [26], metal organic frameworks [27], and porous zeolite structures [8,28], carbon-based nanomaterials are studied till now [29,30]. Lately, there has been a surge in interest in solid monolayers resembling two-dimensional (2D) graphene, such as Si_2BN, due to their potential applications in hydrogen-related advancements [31]. Hydrogen can serve as a viable energy source when adsorbed onto the surface of solid materials, offering safety and cost advantages compared to its gaseous or liquid forms. The use of lighter materials may offer higher gravimetric density, but releasing hydrogen from them under ambient conditions is not as practical due to weaker hydrogen bonding via physical interaction and strong covalent or ionic bonding via chemical interactions. In the coming era, attaining the perfect equilibrium between hydrogen adsorption and monolayer, considering the limits of physisorption and chemisorption, will be crucial for developing efficient hydrogen storage materials [16,32,33]. The materials, which supports physisorption capability of storing hydrogen, are Sorbent Materials. The materials based on carbon; such as nanotubes, graphene, fullerenes, mesoporous silica, isoreticular metal-organic frameworks, metal-organic frameworks (MOFs), covalent-organic frameworks (COFs), and clathrates are sorbent materials [34–37]. However, several challenges limit the effective use of these materials in energy devices. These challenges incorporate a higher desorption temperature, increased likelihood of metal clustering, lethargic uptake and release of hydrogen, and instability at elevated temperatures [16,38]. However, the discovery of graphene [39] has sparked significant interest in 2D materials, renowned for their exceptional strength, outstanding conductivity, expansive surface area, and remarkable chemical and thermal stability [40,41]. There are many 2D systems are studied till now, e.g. Graphene, Borophene, BN, CN, and phosphorene [42–45], 2D materials including MXene Cr_2C [46], Sc_2N MXenes monolayer [47], In_2CO [48] C_2N [45], Ga_2C_6 monolayer [49], B_8S_4Li compounds [50], Li@B_2O [20]. An innovative 2D material honeycomb borophene (h-B_2O) has shown great inspiration of using 2D materials [51]. Recently, a new 2D monolayer B_2CO has been theoretically predicted, demonstrating notable structural, energetic, and kinetic stability [52]. The synthesis techniques for boron and oxygen hybrid graphene are well-established, suggesting that theoretically designed 2D B–C–O materials hold significant potential for practical synthesis [53]. The B_2CO monolayer exhibits semiconductor characteristics, featuring an indirect band gap and displaying both dynamical and energetic stability at temperatures below 300 K. Consequently, being inspired by the exceptional properties of B_2CO monolayer [54], we aimed to explore its potential use as competent and high-performance material to store hydrogen particularly focusing on its reversible qualities along with stability issues. This study aimed to investigate the adsorption properties of H_2 molecules on a pure B_2CO monolayer and assess its potential for hydrogen storage using first-principles calculations grounded in DFT. The findings indicate that B_2CO monolayer meeting the criteria for capacities outlined by the US Department of Energy (6 wt% and 30 g/L) [31]. We also explored the thermal flexibility, electronic characteristics, desorption threshold, charge examination, and energy barrier concerning adsorption process. This work stands out for its detailed analysis of the B_2CO monolayer as a potential material for solid-state hydrogen storage. Its innovation lies in the discovery that this material presents a low energy barrier for hydrogen adsorption, confirmed by CI-NEB analysis, which supports the material's potential for rapid hydrogen uptake. Furthermore, the work extends its novelty by considering the possibility of modifying the material with metal atoms, opening avenues for future optimization. Our findings indicate that the pure B_2CO monolayer exhibits potential as an effective and renewable medium for storing hydrogen with high capacity in the forthcoming hydrogen-based economy.

2. Materials and methods

The calculations were carried out via different modules of Amsterdam density functional (ADF) in the framework of DFT [55–57]. Perdew, Burke, and Ernzerhof (PBE) functional within the generalized gradient approximation (GGA) was utilized to characterize the exchange and correlation effects [58]. The van der Waals (vdW) interactions for long-range correction were included via Grimme method within the framework of DFT-D3 [59]. The basis of the sets encompasses the Triple Zeta Polarization (TZP) basis function, applied without freezing the core [60]. The relativistic effects were not included, as the studied material has low atomic number (Z). The Numerical integration was performed with a convergence threshold set at 1×10^{-5} eV to ensure accuracy. The energy of formation was calculated using equation (1) in order to assess the energetic stability of the monolayer.

$$E_{formation} = \frac{E_{B_2CO} - XE_B - YE_C - ZE_O}{X + Y + Z} \quad (1)$$

Where $E_{formation}$ defines the formation energy for system (B_2CO) per atom, E_{AB} is the total energy of materials of 3x3 slab and, X,Y,Z represent total number of specific atoms (B,C,O) present in a material whereas E_B , E_C, E_O representing the total energies of reactants [61,62].

To calculate the consecutive adsorption energies E_{ads} and average adsorption E_A energy per H_2 molecule for adsorbed B_2CO monolayer, following equations were used.

$$E_{ads} = [(nEH_2 + EB_2CO) - EB_2CO - nEH_2] \quad (2)$$

$$E_A = \frac{1}{n}[(nEH_2 + EB_2CO) - EB_2CO - nEH_2] \quad (3)$$

In case of hydrogen adsorption, E_{ads} is the adsorption energy, E_A is average adsorption energy per H_2 molecule, while variable n denotes

quantity of H_2 molecules, ($nEH_2 + EB_2CO$), EB_2CO, nEH_2 are the collective energies of nH_2 molecules taken by B_2CO monolayer, pure monolayer and single H_2 molecule respectively [63]. In our case, negative value will be the indication of structural stability and consideration of exothermic reaction for the adsorption process [64].

To investigate the influence of thermal effects regarding adsorption and release of H_2 molecules over a pristine B_2CO monolayer, Ab Initio Molecular Dynamics (AIMD) simulations were conducted in NVT statistical ensemble. The number of atoms (N), volume (V), and temperature (T) remained constant while employing MD calculations. In addition to investigate the thermal stability of nH_2@B_2CO, AIMD simulations were carried on B_2CO monolayer in an NVT ensemble while keeping a Nose-Hoover chain thermostat at temperature of 300 K, 450 K, 785 K [65]. The suitability of the B_2CO monolayer for practical hydrogen storage conditions was determined by applying the van't Hoff equation [66,67] to determine the desorption temperature and pressure effects on the adsorbed monolayer as follows:

$$T_D = \frac{E_{ads}}{K_B}\left(\frac{\Delta S}{R} - \ln p\right)^{-1} \tag{4}$$

The symbol E_{ads} denotes the average energy of adsorption per molecule of H_2, while k_B represents the Boltzmann constant ($1.38x10^{-23}$ J/K). The entropy change is denoted by ΔS which is 75.44 J/mol.K for hydrogen gas transition to liquid phase, R denotes the gas constant having value of 8.314 J/mol.K, and p stands for the equilibrium pressure, ranges from 1–10 atm [20].

The effectiveness of material for solid-state hydrogen storage was evaluated by equation (5), which is employed to determine the adsorption capacity in wt% [68,69].

$$wt\,\% = \frac{n \times M\,(H_2)}{n \times M\,(H_2) + M(B_2CO)} \tag{5}$$

The quantity of H_2 molecules is represented by n, where, $M\,(H_2)$ refers to the molecular weight of H_2, and $M(B_2CO)$ denotes the weight of the adsorbed B_2CO monolayer.

The correlation between the nH_2@B_2CO-adsorbed systems, a study was conducted by employing Periodic Energy Decomposition Analysis (PEDA) alongside Natural Orbitals for Chemical Valency (NOCV) calculations on specific geometric configurations. The calculations were conducted by separately analyzing two distinct fragments, yielding multiple energy terms that help elucidate the bonding characteristics of adsorbed molecules within the material [70–72]. The climbing image nudged elastic band (CI-NEB) technique was utilize for deeper understanding of energy barrier associated with hydrogen molecule migration on the host surface [73,74]. The (CI-NEB) improvised form of NEB is used to determine the hydrogen adsorption path along different ways [75,76].

3. Results and discussion

The physical properties and solid-state hydrogen storage mechanism on B_2CO are comprehensively investigated. The findings of the investigations are described in the following sections.

3.1. Structure properties and stability

This study involves investigations on monolayer of B_2CO which has been previously reported and found to be dynamically stable [52]. The assessment for structural integrity of the material, both formation energy and phonon spectra were evaluated, confirming that the material is suitable candidate to investigate storage mechanism. The optimized configuration of the B_2CO monolayer from both top-down and side perspectives is depicted in Fig. 1 (a–c). The formation energy of −1.70 eV, calculated using Eq. (1), indicates that the reaction is exothermic and the structure is energetically stable [77,78]. The energy band diagram shown in Fig. 2 illustrates that material is a semiconductor, with a calculated indirect band gap of 1.62 eV [52]. The B_2CO monolayer has an indirect band gap because the highest point of the valence band (VB) and the lowest point of the conduction band (CB) are not located at the same Gamma (Γ) point. Additionally, Fig. 2 shows the phonon dispersion spectra for 2D monolayer, calculated along the high-symmetry paths of the Brillouin zone (K-M-K). The calculation was performed using a 3 × 3 × 1 supercell, which suggests that the material is both dynamically and kinetically stable, as no negative modes are observed in the spectra [79]. According to our optimization process, for stable minimum state of system, the structure was first fully relaxed in unit cell and to build monolayer a 3x3 supercell was utilized. B_2CO monolayer's unit cell comprises four atoms: one oxygen, one carbon, and two boron atoms [52]. The monolayer B_2CO structure displays a buckled hexagonal lattice, characterized by the space group 156_$P3m1$. The lattice parameters are measured as follows: a = 2.61 Å, b = 2.26 Å, c = 2.61 Å with bond lengths B–C = 1.62 Å, 1.51 Å B–O = 1.60 Å. The dihedral angles B–O–B and B–C–B are found 106.7°,117.6° respectively and these results are persistent with literature [52].

3.2. Adsorption over pristine B_2CO monolayer

This section thoroughly examines the stability and adsorption char-

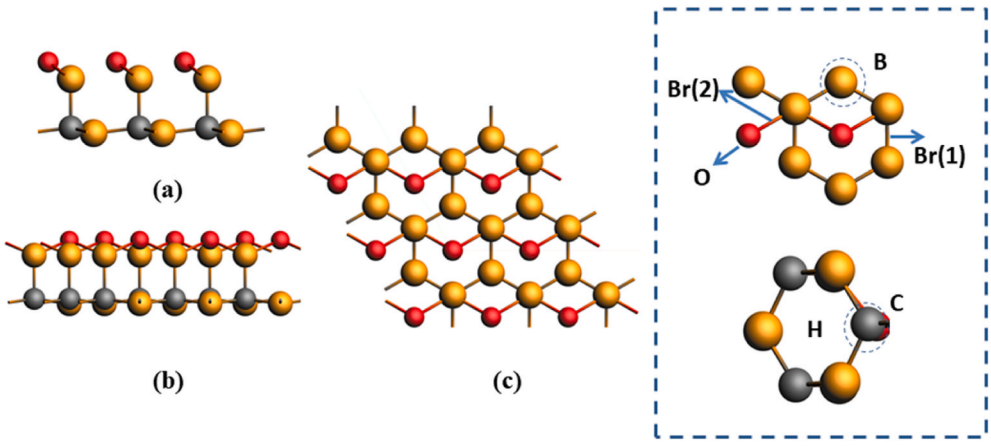

Fig. 1. A 3x3 optimized supercell view along the x-axis (a), y-axis (b), and z-axis (c), where red balls indicating oxygen atoms, grey balls representing carbon atoms and golden balls showing boron atoms. There are six possible adsorption sites such as; boron atom (B), Oxygen (O), bridge 1 (B–B), bridge 2 (B–O) over the top of surface while Carbon (C) and hollow (H) sites downward of surface. (For interpretation of the references to color in this figure legend, the reader is referred to the Web version of this article.)

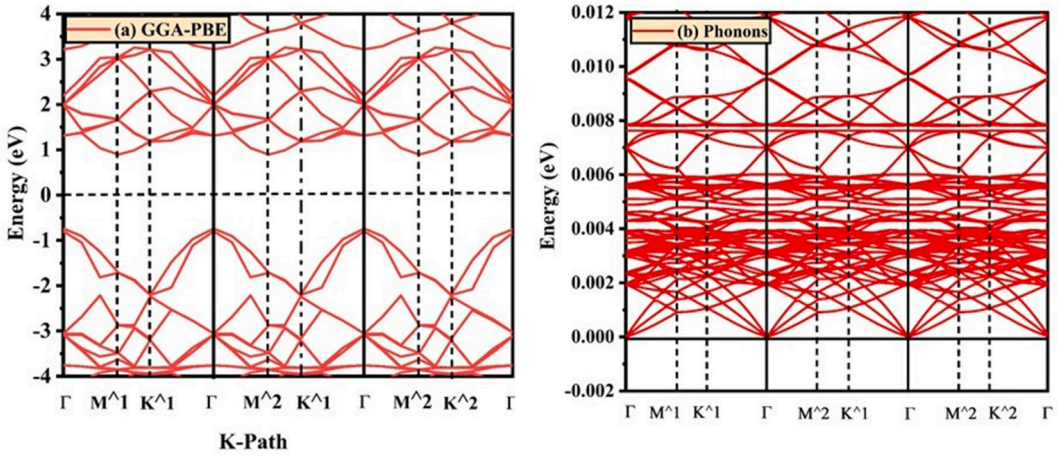

Fig. 2. – The calculated (a) Electronic Band diagram (b) Phonon dispersion curves of pristine B_2CO monolayer.

acteristics when H_2 is adsorbed onto a pristine monolayer, incorporating vdW interactions. We examined the ability of a single H_2 molecule to adsorb onto the pristine B_2CO monolayer in order to assess whether it can effectively capture the H_2 molecule. The potential adsorption sites for H_2 on the B_2CO monolayer were examined, as depicted in Fig. 1 (a–c), such as Boron (B), oxygen (O), bridge 1 (B–B), bridge 2 (B–O) on top of the surface while Carbon (C) hollow (H) at downward side. Hence, by performing single point calculations, it was observed that the adsorption of H_2 at the oxygen site on the top surface and C- site on the downward surface was found out to be most stable configurations. To determine the most stable configuration, we calculated the adsorption energies by placing an H_2 molecule at different potential adsorption sites. Both parallel and vertical orientations relative to the pure monolayer were considered in the analysis. The H_2 molecule demonstrates its closest proximity at 2.82 Å when adsorbed on the O-site and at 1.71 Å. The understanding of how H_2 molecules adhere to the B_2CO monolayer, maximum number of H_2 molecules at favorable adsorption sites were subjected to adsorption for above side and downward of monolayer simultaneously. The stable configurations of these placements are depicted in Fig. 3. The results indicate one side of the monolayer 3x3 size can adsorb $7H_2$ molecules with desired adsorption energies and distances. The adsorption of 8 and 9 molecules on one side of monolayer demonstrated that the distance between the monolayer and H_2 molecules increased to 6.71 Å and 5.32 Å respectively, indicating increased repulsive interactions between adjacent H_2 molecules and surface. Next, we examined the adsorption of H_2 molecules on both surfaces of the B_2CO monolayer. The optimized stable configurations of nH_2 (n = 1–14) molecules adhered to the B_2CO monolayer, encompassing both orientations, are depicted in Fig. 3. It is quite similar to the situation where H_2 molecules were adsorbed on one side of the monolayer. The distance between the B_2CO surface and the 14th adsorbed H_2 molecule is 2.95 Å. This distance notably increased to 6.04 Å upon adsorption of the 15th molecule. These findings point to a situation sketched in Fig. 3 indicating that the surface does not accept the further adsorbed molecules. It points that the monolayer can no longer support further adsorption, demonstrating the saturation. The distance between the adsorbed molecules and the surface ranges from 2.62 Å to 3.34 Å until the saturation point is reached. Beyond this point, the monolayer became overcrowded, leading to increased repulsive interactions between adjacent H_2 molecules due to their close proximity. These repulsions cause the further adsorbed H_2 molecules to shift slightly outward from the surface to minimize the interaction energy, resulting in an increased distance between the molecules and the surface [80]. Because the H atom is kinetically “cold" and cannot overcome the activation barrier of approximately 2.62 Å to 3.34 Å, so it might be trapped above the material’s plane and can only be physiosorbed. This energy barrier represents the amount of energy required for H_2 atoms to move from a free state to a chemisorbed state on monolayer surface [81,82].The assessment of consecutive adsorption energies was carried out by using Eq. (2). The adsorption energy of H_2 molecules on the B_2CO monolayer ranges from (−0.065 to −1.172 e V/H_2), suggesting that H_2 can effectively bind to the surface while negative sign shows the system is capable of storing H_2 molecules spontaneously. This range falls within the adsorption energy range of −0.2 to −0.7 e V/H_2, which is typically associated with physisorption, where the interaction is weak yet stable enough for effective adsorption [7,83]. Additionally, it was observed that as the amount of H_2 molecules absorbed increases, there is a corresponding increase in the level of adsorption energy. Thus, the system can control all absorbed H_2 molecules under typical circumstances. The values enlisted in table-1 shows the successive adsorption energy (E_{ads}), distances between H_2 to B_2CO monolayer (D), the distance between H–H atoms ($d_{H–H}$) and the total charge (Q_H) on absorbed hydrogen atoms for each configurations. This energy barrier represents the amount of energy required for H_2 atoms to move from a free state to a chemisorbed state on monolayer surface [81,82]. The calculated bond length of H_2 molecule is 0.75 Å and bonding energy per atom for isolated H_2 is −3.375 eV which is good agreement with experimental values [84,85]. Furthermore, H_2 molecule maintained its bond length at 0.75 Å, which is the indication of not breaking of their own bond and demonstration of the weak interaction between H_2 molecules and a monolayer, as this is case of non-dissociative interaction predominantly demonstrated by physisorption [16,31]. The Hirshfeld charges (Q_H) in units of ‘e’ computed for the adsorbed hydrogen molecules suggest their proximity to neutrality, signifying that there is no noteworthy transfer of charge from the hydrogen molecules to the B_2CO monolayer, indicating that all the hydrogen molecules are physiosorbed [86]. This neutral behavior is evident in figure S1, where the hydrogen atoms, depicted in white color balls, show charge values of 0.00 on the Hirshfeld charge scale. These findings are consistent with earlier studies on hydrogen storage materials, including those involving functionalized graphene [87,88] and metal-doped B_2C sheet [89]. The calculated average adsorption energy calculated using Eq. (3) in case of 14 hydrogen molecules is - 0.614 eV which is found within the range of reported value of −0.15 eV to - 0.7 eV between the range of physisorption and chemisorption [90]. Furthermore, the negative adsorption energies in Table 1 reflect the formation of stable sites where hydrogen molecules interact electrostatically with the B_2CO monolayer, indicating an exothermic process. As more hydrogen molecules adsorb onto the surface, these interactions become stronger, leading to more negative adsorption energies. This behavior is typical for materials of this kind and further confirms the stability and efficiency of the adsorption process. Additionally, this energy exceeds the physisorption energies of H_2 documented by Bhatia et al. at 0.1

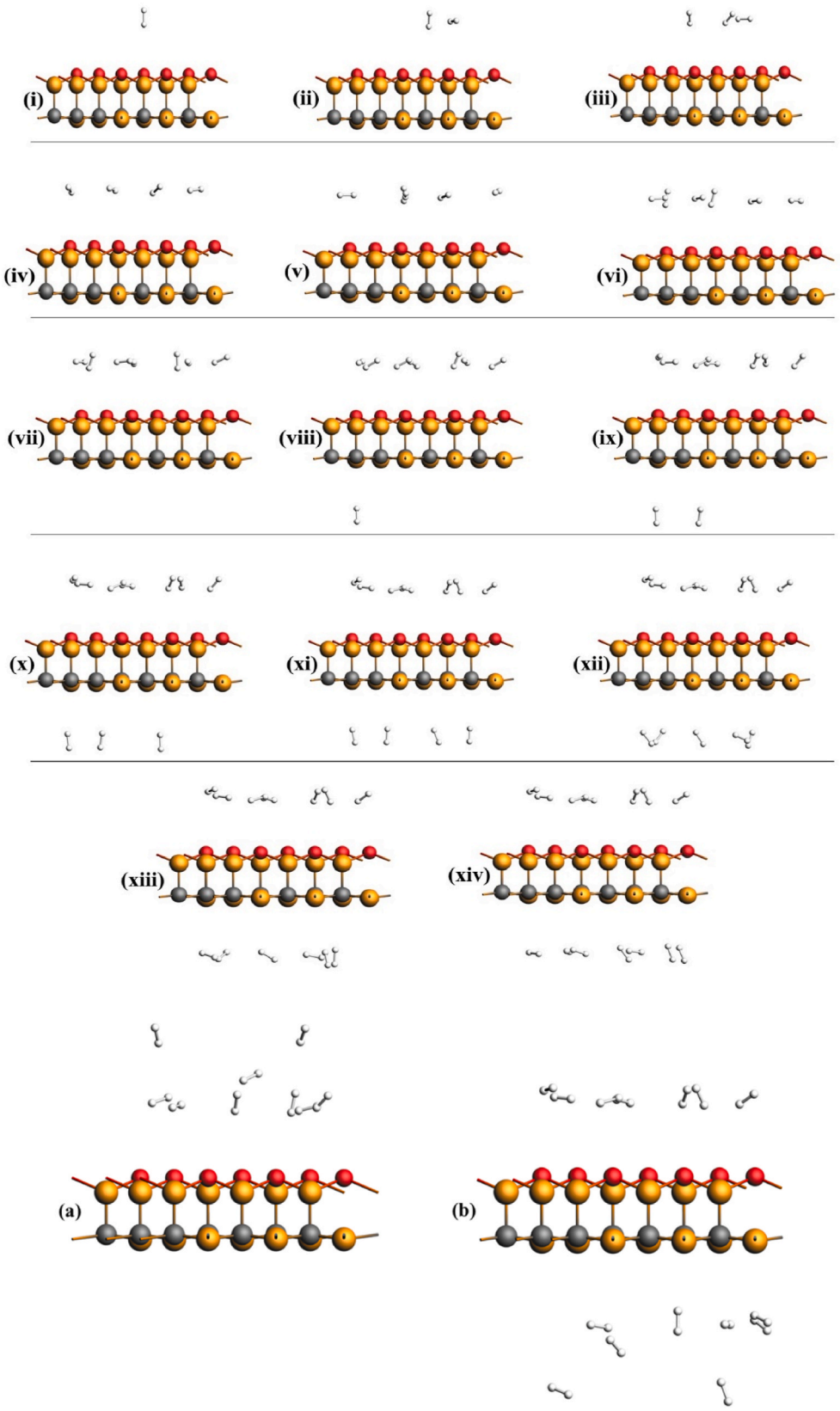

Fig. 3. The side view of optimized stable configurations of (i) $1H_2$, (ii) $2H_2$, (iii) $3H_2$, (iv) $4H_2$, (v) $5H_2$, (vi) $6H_2$, (vii) $7H_2$, (viii) $8H_2$, (ix) $9H_2$, (x) $10H_2$, (xi) $11H_2$, (xii) $12H_2$, (xiii) $13H_2$, (xiv) $14H_2$ adsorbed molecules over B_2CO monolayer respectively. The side view of (a) $9H_2$ and (b) $15H_2$ molecules above and downward of monolayer when excessive molecules are moving away. The white balls are representing H_2 molecules while red, grey, golden balls are showing Oxygen, Carbon and Boron atoms respectively. (For interpretation of the references to color in this figure legend, the reader is referred to the Web version of this article.)

Table 1
The successive adsorption energy (E_{ads}), the distances between H_2 and B_2CO monolayer (D), the distance between H–H atoms (d_{H-H}), Hirshfeld charge analysis (Q_H).

System	E_{ads} (eV)	D (Å)	d_{H-H} (Å)	Q_H (e)
$1H_2@B_2CO$	−0.066	2.62	0.75	−0.022
$2H_2@B_2CO$	−0.144	2.95	0.75	−0.042
$3H_2@B_2CO$	−0.228	2.43	0.75	−0.055
$4H_2@B_2CO$	−0.320	2.40	0.75	−0.063
$5H_2@B_2CO$	−0.408	3.34	0.75	−0.079
$6H_2@B_2CO$	−0.480	2.60	0.75	−0.090
$7H_2@B_2CO$	−0.563	2.54	0.75	−0.101
$8H_2@B_2CO$	−0.648	2.95	0.75	−0.094
$9H_2@B_2CO$	−0.733	3.07	0.75	−0.093
$10H_2@B_2CO$	−0.818	3.24	0.75	−0.090
$11H_2@B_2CO$	−0.914	3.19	0.75	−0.086
$12H_2@B_2CO$	−0.997	3.17	0.75	−0.078
$13H_2@B_2CO$	−1.084	2.91	0.75	−0.071
$14H_2@B_2CO$	−1.172	2.95	0.75	−0.047

eV–0.15 eV at 300 K [84]. Therefore, taking into account all the molecules adsorbed on both sides of the monolayer, the hydrogen storage weight percentage is determined using Eq. (5). This calculation shows that the B_2CO monolayer achieved its theoretical capacity of 5.94 wt%. Further, the volumetric density is estimated by calculating the volume of the monolayer B_2CO and mass of $14H_2$ adsorbed in grams. The volume of a monolayer is calculated by multiplying its basal area by the height, which is the average distance between two layers of hydrogen. The volumetric density of 103 g per liter is determined by dividing the mass of $14H_2$ molecules by the specified volume, and this result aligns with values found in the existing literature [88,91]. The obtained gravimetric and volumetric capacities are as per requirements to the ideal recommended target of 6 wt% and 30 g/L [87,92,93]. The extended D (Å) measurements and the consistent d_{H-H} (Å) values may suggest that the hydrogen molecule adsorbed weakly onto the pristine B_2CO monolayer [94]. Moreover, adsorption on both sides of the B_2CO monolayer is more advantageous when practical application of the material is considered. The findings indicate effectively doubling the adsorption sites thus enabling a higher hydrogen storage capacity of $14H_2$ molecules as compared to $7H_2$ molecules on a single side. This increases gravimetric and volumetric densities, crucial for practical applications. Additionally, a balanced distribution of adsorbed molecules reduces localized strain, preserving structural integrity and enhancing reversibility during hydrogen cycles. Utilizing both sides also optimizes active site usage, ensuring efficient adsorption without destabilization. These factors make dual-sided adsorption more suitable approach for real-world hydrogen storage systems.

In the physiosorbed state, the bond length in the molecule H_2 typically remains close to its gas-phase value of about 0.74 Å. In our study, H–H bond length showed no significant change and remained at 0.75 Å, confirming the physisorption nature of the interaction. Hence, the absence of H_2 dissociation or bond breakage to form a hydrogen bond with the surface, observation of a typical H–H bond length, and the weaker adsorption energy point to physisorption of H_2 molecules on B_2CO monolayer.

3.3. Desorption temperature and thermal stability

The desorption temperature is computed to assess a material's capability to release hydrogen for practical applications. The ability to release H_2 molecules reversibly under normal conditions is equally essential for storage related applications. Typically, as the adsorption energy increases, the temperature at which H_2 molecules desorb (T_D) also rises and it can be estimated by using average adsorption energy. In this study, the average adsorption energy measured using Eq. (3) for the system comprising 14 hydrogen molecules is −0.614 eV, indicating a potentially suitable value for material supporting physisorption. The T_D for all H_2 molecules, which are adsorbed on pristine B_2CO, is calculated by utilizing value of average adsorption energy in van't Hoff's equation [21,95,96]. The findings indicate that the average operating temperature for T_D is approximately 785 K, notably greater than room temperature and well suited for real-world fuel cell utilization. To assess the suitability of B_2CO monolayer for practical hydrogen storage, we conducted the analysis of the thermal stability for the system both pre- and post-adsorption. This evaluation aimed to gauge the system's resilience at ambient temperature. The evaluation of thermal stability to assess the T_D and withstand temperature of B_2CO monolayer, AIMD simulations were carried out using a 3x3 supercell within an NVT ensemble. The Nose-Hoover Chain thermostat was employed to ensure temperature stability throughout the simulations. The $3 \times 3 \times 1$ size of B_2CO with and without adsorption of hydrogen molecules was equilibrated for setting a time step of 0.25 fs using 100000 number of steps in AIMD simulations [97,98]. At first, the stability for pristine material was checked by running MD calculations at 300 K. The MD plot illustrates the temperature and energy of the pristine material over specified time intervals, as depicted in figure S2 (a-c). The graph in figure S2 (a) indicates that after 5 ps, the overall energy of the structure remains stable. This observation suggests that the structure remained intact without any deformation or bond breakage. The snapshots of pristine B_2CO monolayer along z-axis from initial to 15 ps changes are shown in Fig. S2 (b & c) as a function of time. This proposes that B_2CO exhibits excellent thermal stability and is a suitable choice for storage media. Fig. 4 (a, b) shows the MD plots of temperature and energy of the hydrogenated material along with corresponding snapshots at 5 ps intervals. The inclusive energy of the material remains relatively stable [99] as seen from Fig. 4 (a). The snapshots in Fig. 4 (b) are captured at intervals of 5 ps and this data suggests that following a period of 5 ps, the total energy of the structure remains relatively stable. The snapshots for H_2 adsorbed pure B_2CO monolayer along z-axis from initial to 25 ps changes as a function of time, depicting that system remain intact. These pictorial representations are consistent with graph showing energy equilibrium. Additionally, Fig. 5(a and b) displays the MD plots of the hydrogenated material at temperatures of 450 K and 785 K, illustrating the specified time intervals. The system also exhibited stability at a temperature of 450 K in Fig. 5 (a), maintaining equilibrium even after being subjected to room temperature conditions (300 K). However, signs of distortion began to emerge as the temperature increased to 700 K up to theoretically evaluated desorption temperature (785 K) as depicted by Fig. 5 (b). By the time, the temperature reached 785 K, the system's energy ceased to remain constant and all the hydrogen molecules escaped through system. According to these, AIMD findings, B_2CO monolayer can effectively captures H_2 molecules at 300 K up to 450 K; however, as the temperature rises, majority of the H_2 molecules will leave the material due to thermal effects. The thermal effects became more pronounced at elevated temperature and the increased thermal energy leads to greater kinetic motion of the H_2 molecules, causing them to overcome the binding forces with the monolayer. In order to count the pressure effects for the desorption, we applied van 't Hoff's equation over a pressure range of 1–10 atm, using the average adsorption energy to determine the conditions necessary for the complete desorption of molecules from the surface. Therefore, all T_D (p) dependencies were obtained by employing hydrogen adsorption energy for $14H_2@B_2CO$. Fig. 5(c) presents the correlation between desorption temperature (T_D) and varying equilibrium pressures to highlight the mechanism of desorption at higher temperatures with an increase of pressure. At elevated pressures, the release of further hydrogen molecules typically requires higher temperatures due to the difficulty of desorbing more molecules against the increased gas pressure. Hence, the moderate temperature and low pressure, such as 1 atm, provide the suitable conditions for optimal hydrogen desorption. The observed behavior of desorption temperatures as a function of pressure in this situation show agreement with previously reported trend [65,68]. The pressure-dependent behavior highlights the importance of considering the thermal effects when assessing

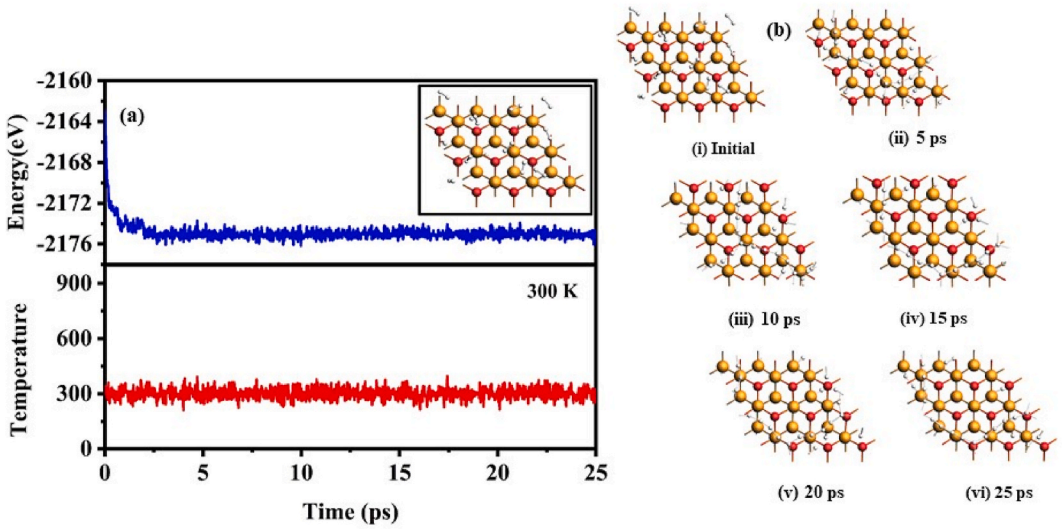

Fig. 4. AIMD calculations of (a) hydrogenated monolayer for n = $14H_2$ at 300 K, (b) Snapshots of adsorbed system B_2CO along z-axis as a function of time as considered from MD simulations.

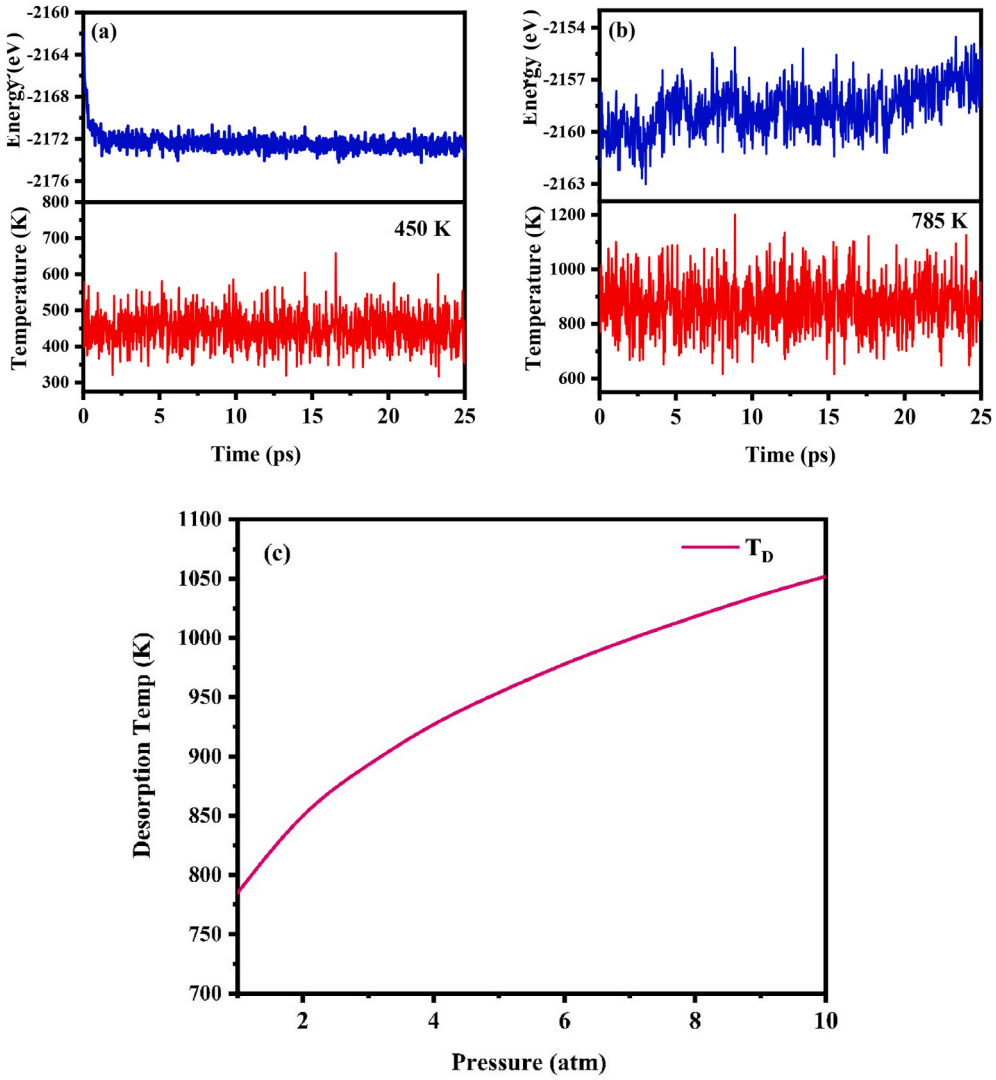

Fig. 5. AIMD calculations of hydrogenated monolayer for (a) $14H_2$ at 450 K (b) $14H_2$ at 785 K and (c) correlation between desorption temperature, binding energy and equilibrium pressure up to 10 atm.

the stability and performance of solid state hydrogen storage or other applications involving molecular adsorption [66]. Therefore, it is concluded that the structure of B_2CO with the highest amount of adsorbed hydrogen remains stable at 300 K and indicate the material's durability under room temperature conditions. This shows the material has ability to hold hydrogen molecules without any distortion at room temperature and it fulfils the requirement of best storage media.

3.4. ELF analysis

The analysis of ELF plots is another method for investigating a qualitative change in charge transfer parameters [95,100]. The ELF function contains values ranging from 0–1, which specify the regions of electronic distribution in a system. The value of 0 denotes electron delocalization, while 1 signifies electron localization. An ELF value of 0.5 suggests that the material has a balanced distribution of both localized and delocalized electronic densities [95,101]. The behavior of pristine material is observed from Fig. 6 (a - f), as there are two electron regions where localization is present in B_2CO monolayer. The region one is around O atoms, while the C atoms form another surrounding structure. In contrast, the ELF value for the B atom is below 0.5, indicating that its electron density is more localized. The overlapping of charge densities between H_2 molecules and material is also illustrated through drawing ELF diagrams as shown in Fig. 6 (a - f) for nH_2-B_2CO systems. It is clear from the representative plots that there is delocalized region between nH_2 molecules and B_2CO monolayer, indicating the absence of covalent bonding between nH_2-B_2CO. As a result, these findings indicate that the electron clouds surrounding H_2 molecules imply a lack of orbital interactions between the H_2 molecules and any atoms within the host monolayer [102]. Thus, the bonding between nH_2 and B_2CO is attractive in nature due to vdW electrostatic interactions, as there is no exchange of charges occurring between the surface and the hydrogen, leading to a mild level of attachment [103]. This is the indication for non-dissociative kind of adsorption, which is actually a characteristic of physiosorbed system, favoring reversibility of H_2. The adsorption of H_2 molecules appears to have no impact on the binding interactions between the B, C, and O atoms in the monolayer. Therefore, based on the analysis from ELF plots, it is predicted that phenomenon of adsorption is of physiosorbed nature.

3.5. Electronic properties

The analysis of total electronic densities (TDOS) and the PDOS is constructed to better understand the interactions before and after adsorption of total hydrogen molecules for B_2CO system. To comprehend the behavior of pure B_2CO, the electronic characteristics of both the pristine and adsorbed configurations are computed. The pristine monolayer behavior is depicted by figure S3 (a,b), further TDOS and PDOS data clearly indicate that the primary contribution comes from the p orbitals of O and C in valence band maximum (VBM) and boron p orbitals in conduction band minimum (CBM) of the monolayer. The influence of hydrogen adsorption over monolayer PDOS of different H_2.absorbed systems is depicted in Fig. 7(a–d). The analysis of PDOS reveals that hydrogen molecules adsorbed on the B_2CO monolayer create low-energy states within the −4 to −6 eV range. This recommends that the presence of adsorbed hydrogen molecules contributes minimal influence on the interactions among atoms of boron, carbon, and oxygen in the B_2CO monolayer [104,105]. Moreover, by examining Fig. 7(a–d), it becomes clear with an increased adsorption of molecules, the peak of H_2 becomes more prominent in the energy states of the pristine material. This indicates an enhanced interaction between H_2 and B_2CO; however, it demonstrates a feeble hybridization between the hydrogen s orbital and the B_2CO orbitals positioned approximately at −6 eV energy level [66]. This type of weak orbital hybridizations has been identified in alternative nanomaterials used for hydrogen storage [106–108]. The observations showed that, there is negligible alteration between the VB and CB for the material following adsorption. These findings are in agreement with the ELF results, which also indicate that the presence of H_2 molecules does not influence the bonding interactions among the atoms in the monolayer. The earlier discussion indicates that electrostatic forces drive the primary interactions between the H_2 and B_2CO monolayer.

3.6. PEDA-NOCV analysis

The characteristics of the surface bond were acquired through peri-

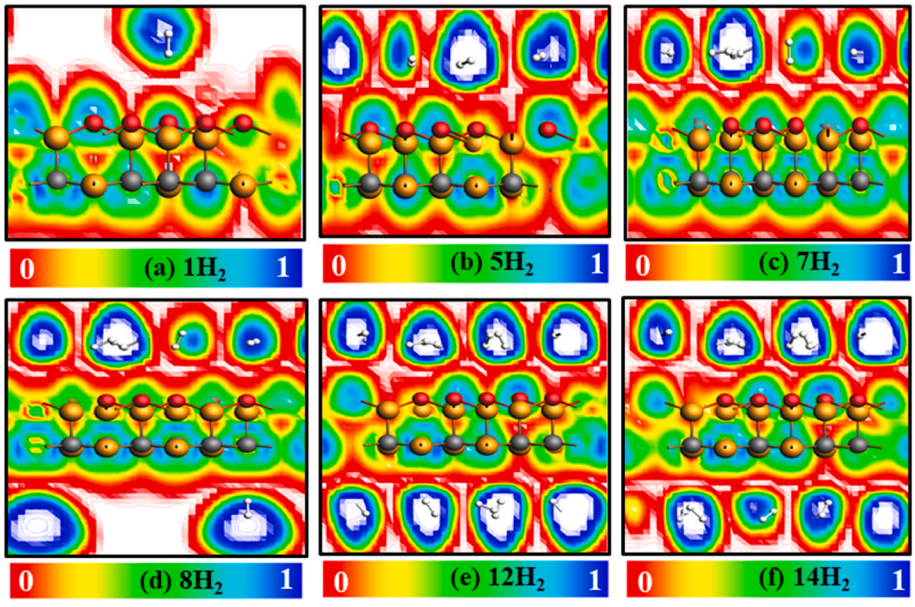

Fig. 6. Electron localization function plots of B_2CO monolayer with (a) $1H_2$ (b) $5H_2$ (c) $7H_2$ (d) $8H_2$ (e) $12H_2$ (f) $14H_2$. The configurations consist of white atoms symbolizing H_2 molecules, golden balls representing boron atoms, red balls indicating oxygen atoms, and grey balls denoting carbon atoms. The scale provided represents charge density, where red indicates a low charge density with a value of 0, while blue indicates electron localization with a value of 1. (For interpretation of the references to color in this figure legend, the reader is referred to the Web version of this article.)

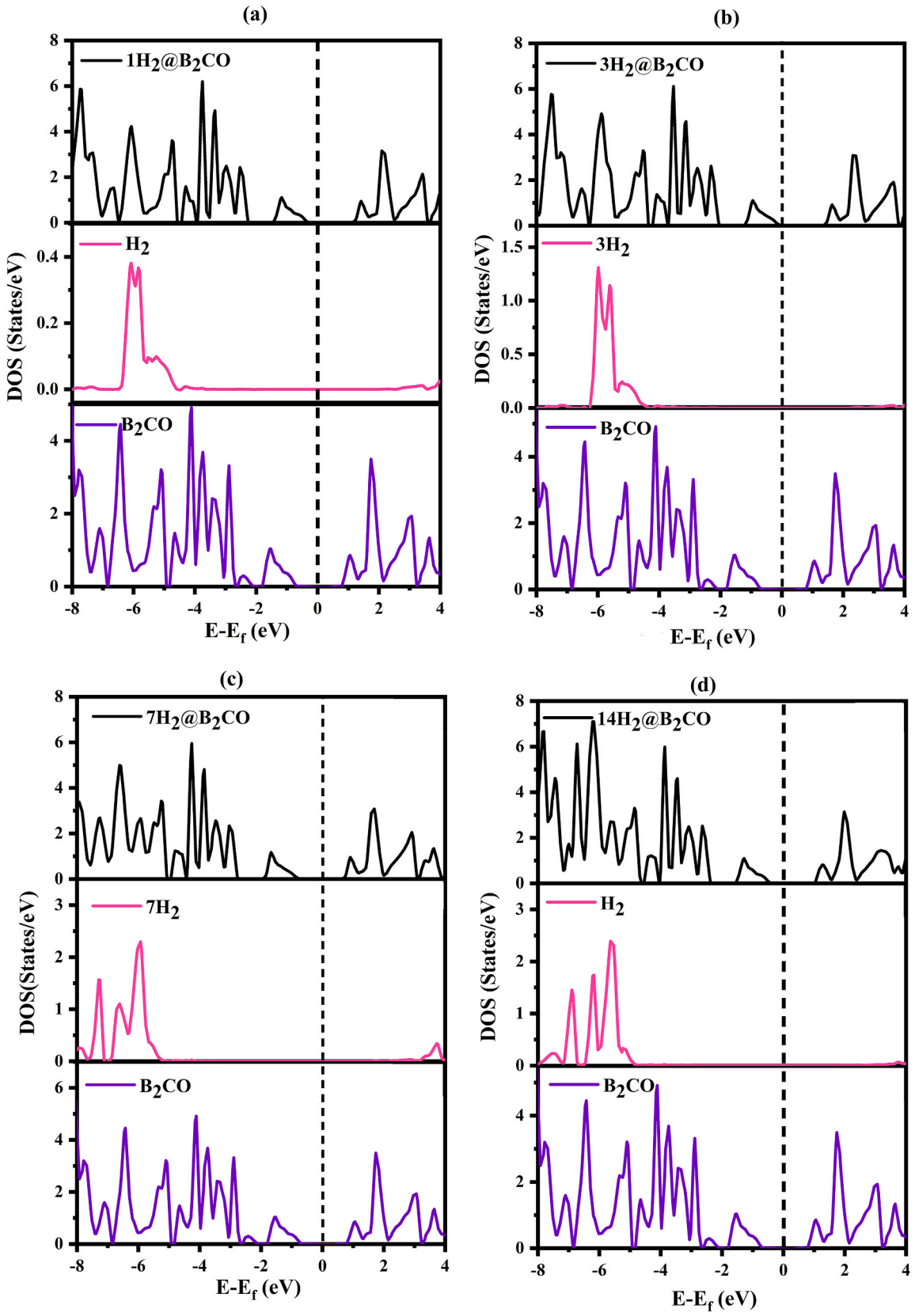

Fig. 7. The calculated total DOS for (a) $1H_2@B_2CO$, (b) $3H_2@$ B_2CO, (c) $7H_2@$ B_2CO, and (d) $14H_2@$ B_2CO. For each system, the DOSs of adsorbed H_2 molecules on B_2CO monolayer, the figures depict H_2 molecules at the top, pure monolayer B_2CO in the middle, and B_2CO at the bottom. The energy of the Fermi level is designated as zero.

odic energy decomposition analysis (pEDA) conducted at the PBE-D3 theory level. This approach involves partitioning the adsorbate structure into two components: one comprising the molecule and the other representing the surface, indicated by Fig. S4. Moreover, the overall interaction energy is categorized into various components, highlighting the specifics of the bonding between the surface and the adsorbate [109]. The interaction energy (IE) results from the interaction between the two fragments when they come into contact within their complex arrangement [110–112]. The equation below can be used to calculate the IE:

$$IE = E_{XY} - (E_x + E_Y) \tag{6}$$

E_{XY} represents the energy of the complex, while E_x and E_Y denotes energies of individual fragments e.g. X and Y within the complex. The IE can be divided into different energy constituents, as described below.

$$\mathrm{IE} = \Delta E_{\mathrm{Pauli}} + \Delta E_{\mathrm{elstat}} + \Delta E_{\mathrm{orb}} \tag{7}$$

$\Delta E_{\mathrm{steric}}$ is the steric energy component

$$\Delta E_{\mathrm{steric}} = \Delta E_{\mathrm{elstat}} + \Delta E_{\mathrm{Pauli}} \tag{8}$$

The term $\Delta E_{\mathrm{Pauli}}$ refers to the Pauli energy, which results from the exchange repulsion between fragments, in accordance with the Pauli Exclusion Principle. The term $\Delta E_{\mathrm{elastat}}$ represents the quasiclassical electrostatic interaction energy between the charge densities of the specified regions. Furthermore, orbital energy ΔE_{orb} increases as a result of the mixing of orbitals. The value of Pauli energy acts as a destabilizing factor, while electrostatic energy $\Delta E_{\mathrm{elstat}}$ serves as a stabilizing factor [110–112]. The components, $\Delta E_{\mathrm{elstat}}$ and $\Delta E_{\mathrm{Pauli}}$ combine to constitute the steric energy. Table 2 presents the values for all absorbed hydrogen molecules and their interaction energies, which are evaluated using the following terms. The results obtained from the pEDA analysis, Pauli component that is a repulsion measurement, falls within the energy range of 0.035–0.541 eV. The electrostatic energy component ranges from −0.023 to −0.256 eV. A key observation is that the destabilizing Pauli component is greater in magnitude than the stabilizing electrostatic component. As a result, the combined effect of the Pauli and electrostatic energy components leads to an unstable steric component. The stability of the systems is mainly determined by the orbital contribution, which consistently promotes stabilization. This is because the change in ΔE_{orb} is always attractive, as shown in Table 2. The increase in orbital energy from $1H_2$–$14H_2$ enhances the stability of nH_2 on B_2CO. It is crucial to highlight that the stabilizing orbital aspect surpasses the weakening steric element, with its values ranging from −0.022 to −0.221 eV. Therefore, Interaction energies in our study refer to the strength of interactions between atoms or molecules of a whole system or complex. They assess the energy changes associated with these interactions and help determine whether they are attractive (bonding) or repulsive (non-bonding) [113]. The observations from pEDA analysis showed that all the nH_2-B_2CO complexes examined in this study exhibit favorable energy stability and the interaction energies between nH_2 and B_2CO monolayer lie in the range of (−0.063 to −0.779 eV).

Table-2
Interaction energies of n hydrogen molecules adsorbed- B_2CO surface, along with the various energy factors that contribute to the IE.

n	$\Delta E_{\mathrm{pauli}}$ (eV)	ΔE_{disp} (eV)	$\Delta E_{\mathrm{elstat}}$ (eV)	$\Delta E_{\mathrm{staric}}$ (eV)	$\Delta E_{\mathrm{orbital}}$ (eV)	*IE* (eV)
1	0.035	−0.053	−0.023	0.012	−0.022	−0.063
2	0.093	−0.125	−0.057	0.036	−0.039	−0.128
3	0.117	−0.185	−0.071	0.046	−0.050	−0.188
4	0.159	−0.249	−0.097	0.062	−0.055	−0.242
5	0.206	−0.306	−0.113	0.094	−0.072	−0.285
6	0.219	−0.349	−0.119	0.100	−0.083	−0.332
7	0.267	−0.406	−0.136	0.131	−0.097	−0.373
8	0.299	−0.471	−0.156	0.142	−0.123	−0.452
9	0.345	−0.534	−0.177	0.168	−0.155	−0.521
10	0.374	−0.594	−0.185	0.188	−0.182	−0.588
11	0.429	−0.660	−0.212	0.216	−0.211	−0.654
12	0.469	−0.723	−0.231	0.238	−0.211	−0.696
13	0.526	−0.790	−0.256	0.270	−0.216	−0.736
14	0.541	−0.843	−0.256	0.285	−0.221	−0.779

3.7. Energy barrier- NEB plots

The CI-NEB method was utilized to evaluate the energy barrier, which determines the amount of energy required for the transition state from reactants to products. This barrier is assessed through complete examination of the energy profile obtained by NEB simulations [74,119]. The energy barrier for the reaction process is determined by computing the variance between the most energetically demanding state and the least energetically demanding state. This approach offers in-depth understanding into the complex mechanisms underlying chemical reactions [75]. The images of NEB simulations allow us to find the most favorable pathways for hydrogen adsorption, desorption, or diffusion and help us design storage materials and factors that improve the speed of hydrogen absorption and release. The energy barriers profiles are presented in Fig. 8(a–f) along all possible axes above and below side of the monolayer. The observed values for the top side of monolayer are 0.002 eV, 0.003 eV, 0.003 eV along 8 (a) x, 8 (b) y, 8 (c) z path respectively. It is clear from the calculated values that H_2 molecule faces a negligible barrier while storing into material for all 3-path ways, as all values show no noticeable difference. The measurements for the lower energy range of the monolayer are 0.007 eV, 0.006 eV, and 0.006 eV along the paths represented by 8 (d) x, 8 (e) y, and 8 (f) z, respectively, as illustrated in Fig. 8. Therefore, based on the computed values, it is evident that the H_2 molecule encounters an insignificant barrier during storage within the material for all three pathways, as all the values indicate a lack of significant variation. The values of activation dynamics for both adsorption and desorption are crucial in determining the kinetics of a system. While adsorption occurs without any energy barrier, desorption involves overcoming a significant energy barrier [120].

3.8. Monolayer decoration

The process of adsorbing foreign atoms and molecules onto graphene shows great promise as it allows for controlled modifications to the pure material structure [50,116,121,122]. However, there are numerous exceptional hydrogen storage materials that have been created and synthesized through the utilization of metal decoration, which include metal@nanoclusters [123–125] metal hydride complexes [126,127] metal@organic molecules structures [127,128] metal-organic frameworks (MOFs) [129,130], metal@carbon-based materials including graphene [94], metal@boron-based materials including Borophene [131]. Hence, we also examined the modification properties of the monolayer by decorating it with Li, Na, Mg, Ti, V, Sc, Pd, and Mo atoms respectively. The results demonstrated that the monolayer modification with Li, Na, Mg is energetically favorable, whereas modification with Ti, V, Sc, Pd, Mo does not favor energetic stability. These forthcoming results are expected to illustrate the possibility of decorating the monolayer with Li, Na, and Mg metals.

3.9. Comparison with experimental study

From experimental aspects, much research on the reversible hydrogen sorption of carbon nanostructures has been conducted [132,133]. These studies indicate that the electrochemical absorption of hydrogen is reversible [134–136]. The research on various carbon materials, such as activated carbon, carbon nanohorns, carbon nanotubes, and graphitic carbon nanofibers, demonstrated that their weight % ranged below 1 wt% at both room temperature and liquid nitrogen temperature (77 K). However, when the adsorption temperature is

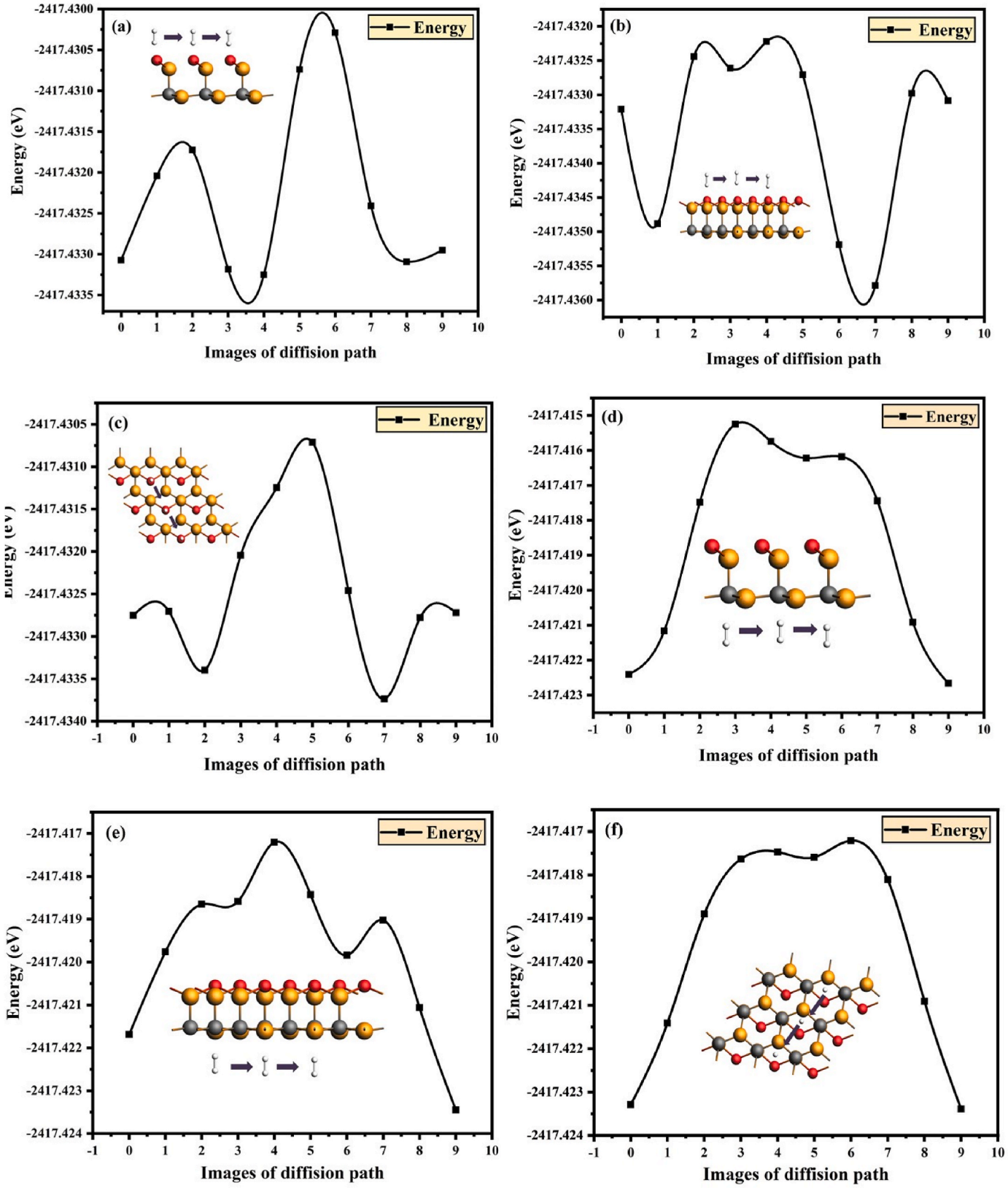

Fig. 8. The calculated Cl-NEB simulation migration pathways for H_2 in the host B_2CO in slab periodicity along the x-axis (above) with energy-barrier 0.002 eV (b) along y-axis (above) with energy-barrier 0.003 eV (c) along the z-axis (above) with energy-barrier 0.003 eV, along the x-axis (below) with energy-barrier 0.007 eV (b) along y-axis (below) with energy-barrier 0.006 eV (c) along the z-axis (below) with energy-barrier 0.006 eV.

reduced to 77 K, the hydrogen storage capacity notably increases, reaching up to 5.7 wt% at a pressure of 3 MPa [137]. While this study demonstrates that the hydrogen uptake capacity for B_2CO monolayer is calculated to be approximately 5.94 wt% at room temperature, which is greater than that of experimentally measured values for carbon materials at room temperature. The DFT calculations suggested an alternative reaction pathway, showing that hydrogen atoms tend to chemically bond with the outer surface of a nanotube [138,139]. There is a possibility of atoms migrating and recombining into hydrogen molecules within the nanotube cavity, forming a concentric cylinder when coverage is high. However, if there is a lower likelihood of chemisorption compared to hydrocarbons, the amount of hydrogen absorbed is directly related to the surface area of the carbon sample and can be released at a relatively positive electrochemical potential. Thus, the maximum hydrogen uptake of a material can be predicted based on the amount of hydrogen accommodated on a single monolayer [140].

In physisorption, the process is driven by van der Waals forces. These forces arise due to the resonant fluctuations in the charge distribution between gas molecules and solid surfaces. This interaction energy is considered as London Dispersion forces, between a substrate (S) and a hydrogen molecule (H_2) is described by.

$$E_{s-H_2} = \frac{\alpha_{H2}\alpha_s}{R^6} \tag{9}$$

The symbol α stands for polarizability, while R represents the distance involved in the interaction. Since αH_2 is constant, enhancing E_{s-H_2} can only be achieved by utilizing substrates with high polarizability, such as those featuring electron systems. The theoretical weight percentage capacity can be determined by examining the material's specific surface area, as the amount of hydrogen it can adsorb is directly proportional to this characteristic. The experiments have shown that activated carbon possess comparatively large surface area compared to bulk graphite, thus making practical hydrogen uptake unobservable [141]. The experimental relationship between high surface area and theoretical capacity exhibited a direct correspondence. Thus, these experiments and assumptions suggest that utilizing a B_2CO monolayer substrate instead of its bulk form would offer a practical means to achieve hydrogen storage as best storage media. Below is Table 3, presenting the theoretical capacities of various materials studied in the literature, along with a comparison to the material we have investigated. This comparison highlights key differences and similarities in performance, offering a comprehensive view of how our material stands relative to others in terms of theoretical properties.

Table-3
Comparison with other reported solid state hydrogen storage systems for theoretical capacity (wt%), desorption temperature (K), average adsorption energy (eV/H_2).

Sr. no	Systems	Theoretical Storage capacity	Desorption temperature (K)	Average adsorption energy (eV/H_2)
1	nH_2@B_2CO (This study)	5.94 wt% 103 g/L	785	−0.614
2	nH_2@C_7N_6 [63]	11.1 wt% 169 g/L,	239	−0.202
3	nH_2@TiZrVMoNb [114]	2.65 wt%	–	−1.120
4	nH_2@Y-pours graphene [115]	7.87 wt%	–	−0.230
5	nH_2@$Li_{12}C_{60}$ [103]	9 wt% 70 g/L	–	−0.075
6	nH_2@La_3B_{18} [66]	5.6 wt%	211	−0.129
7	nH_2@B_4C_3 [116]	6.22 wt%	269	−0.232
8	nH_2@ Sc-biphenylene [65]	11.07 wt%	305	−0.412
9	nH_2@ $C_{48}B_{12}$ [117]	7.1 wt%	–	−0.240
10	nH_2@ Ti–MoS_2 [118]	5.93 wt%	–	−0.472

The findings of this study highlight prospects to enhance the material's performance and applicability for hydrogen storage. To improve the material's performance, a potential approach could involve decorating the B_2CO monolayer with metal atoms, a method commonly used in modern materials research. This modification could potentially enhance hydrogen adsorption energies, improve storage capacities, and optimize desorption conditions. Metal functionalization has been a proven strategy in similar studies to tailor the electronic and structural properties of materials. The experimental validation of the theoretical predictions is crucial to solidify the viability of the B_2CO monolayer in practical applications. The conventional synthesis methods, including chemical vapor deposition may be utilized to fabricate pristine B_2CO monolayer and its metal decorated counterpart. The scalability of the B_2CO monolayer for industrial applications warrants investigation. The studies focusing on the material's behavior under high-pressure hydrogen environments, long-term cycling stability, and integration into storage systems are essential to bridge the gap between laboratory-scale research and commercial deployment. Finally, exploring the material's compatibility with hybrid systems, such as combining B_2CO with other high-capacity storage materials, could unlock synergies that boost overall performance. This approach may also mitigate challenges like material degradation or limited reversibility in practical scenarios.

4. Conclusion

The first-principles calculations were carried out to investigate the potential of pristine B_2CO monolayer for solid-state hydrogen storage. The study revealed that H_2 molecules spontaneously adsorb onto the B_2CO monolayer, exhibiting adsorption energies between −0.066 eV and −1.712 eV with a suitable average adsorption energy −0.614 eV. The interactions of H_2 with the monolayer were identified as electrostatic in nature, explained through DOS and ELF plots while analyzing adsorption study. The material demonstrated hydrogen storage capacities of 5.94 wt% by weight and 103 g/L by volume. The reversibility of material was ensured by predicting its desorption temperature to be 785 K, crucial for assessing dehydrogenation. This temperature estimate indicates that the B_2CO monolayer has the potential to serve as an effective and reversible hydrogen storage medium under real-world conditions. The high desorption temperature of 785 K in solid-state hydrogen storage offers the advantage of controlled hydrogen release. It also ensures controlled hydrogen release, making it suitable for high-temperature industrial applications such as fuel cells and chemical reactors. Additionally, the pEDA analysis verified the presence of favorable interactions between the H_2 molecules and the material. Notably, simulation plots from CI-NEB analysis indicated a remarkably low energy barrier during the hydrogen adsorption process, further supporting the material's potential. The study's findings highlight the potential of the B_2CO monolayer as a strong contender for hydrogen storage. It demonstrates an efficient, reversible, and significant storage capacity, making it suitable for practical applications.

CRediT authorship contribution statement

Rushba Zulfiqar: Writing – original draft, Investigation, Formal analysis, Data curation. **Abdul Majid:** Supervision, Methodology, Conceptualization. **Mohammad Alkhedher:** Visualization, Validation, Methodology. **Sajjad Haider:** Visualization, Validation, Methodology. **Kamran Alam:** Visualization, Validation, Methodology. **Salahuddin Khan:** Visualization, Validation, Methodology.

Ethical Approval

Not applicable.

Availability of data and materials

Not applicable.

Funding

The authors sincerely appreciate funding from Researchers Supporting Project number (RSP2025R399), King Saud University, Riyadh, Saudi Arabia.

Declaration of competing interest

The authors declare that they have no known competing financial interests or personal relationships that could have appeared to influence the work reported in this paper.

Appendix A. Supplementary data

Supplementary data to this article can be found online at https://doi.org/10.1016/j.ijhydene.2025.02.322.

References

[1] Yang, J, et al. High capacity hydrogen storage materials: attributes for automotive applications and techniques for materials discovery. Chem Soc Rev 2010;39(2):656–75.
[2] Mazloomi K, Gomes C. Hydrogen as an energy carrier: prospects and challenges. Renew Sustain Energy Rev 2012;16(5):3024–33.
[3] Glenk G, Reichelstein S. Economics of converting renewable power to hydrogen. Nat Energy 2019;4(3):216–22.
[4] Abe JO, et al. Hydrogen energy, economy and storage: review and recommendation. Int J Hydrogen Energy 2019;44(29):15072–86.
[5] Amica G, Larochette PA, Gennari FC. Light metal hydride-based hydrogen storage system: economic assessment in Argentina. Int J Hydrogen Energy 2020;45(38):18789–801.
[6] Li Y, et al. Graphene confined MoS2 particles for accelerated electrocatalytic hydrogen evolution. Int J Hydrogen Energy 2019;44(16):8070–8.
[7] Satyapal S, et al. The US department of energy's national hydrogen storage Project: progress towards meeting hydrogen-powered vehicle requirements. Catal Today 2007;120(3–4):246–56.
[8] Niaz S, Manzoor T, Pandith AH. Hydrogen storage: materials, methods and perspectives. Renew Sustain Energy Rev 2015;50:457–69.
[9] Hirscher M. Handbook of hydrogen storage. Top Appl Phys 2010;12.
[10] de Bruijn FA. In: Züttel Andreas, Borgschulte Andreas, Schlapbach Louis, editors. Hydrogen as a future energy carrier. Wiley Online Library; 2008.
[11] Abdalla AM, et al. Hydrogen production, storage, transportation and key challenges with applications: a review. Energy Convers Manag 2018;165:602–27.
[12] Usman MR. Hydrogen storage methods: review and current status. Renew Sustain Energy Rev 2022;167:112743.
[13] Allendorf MD, et al. An assessment of strategies for the development of solid-state adsorbents for vehicular hydrogen storage. Energy Environ Sci 2018;11(10):2784–812.
[14] Langmi H, et al. Hydrogen adsorption in zeolites A, X, Y and RHO. J Alloys Compd 2003;356:710–5.
[15] Hassan I, et al. Hydrogen storage technologies for stationary and mobile applications: review, analysis and perspectives. Renew Sustain Energy Rev 2021;149:111311.
[16] Jena P. Materials for hydrogen storage: past, present, and future. J Phys Chem Lett 2011;2(3):206–11.
[17] Newns D. Self-consistent model of hydrogen chemisorption. Phys Rev 1969;178(3):1123.
[18] Hashmi A, et al. Ultra-high capacity hydrogen storage in a Li decorated two-dimensional C 2 N layer. J Mater Chem A 2017;5(6):2821–8.
[19] Liu H-Y, et al. 2D AlP3 with high carrier mobility and tunable band structure. J Phys Condens Matter 2019;32(5):055001.
[20] Gao F, et al. Li-decorated B2O as potential candidates for hydrogen storage: a DFT simulations study. Int J Hydrogen Energy 2021;46(67):33486–95.
[21] Kumar S, Sathe RY, Kumar TD. Sc and Ti-functionalized 4-tert-butylcalix [4] arene as reversible hydrogen storage material. Int J Hydrogen Energy 2019;44(25):12724–32.
[22] Cieslik J, Kula P, Sato R. Performance of containers with hydrogen storage alloys for hydrogen compression in heat treatment facilities. J Alloys Compd 2011;509(9):3972–7.
[23] Heung LK. Using metal hydride to store hydrogen. United States: Department of Energy; 2003.
[24] Sakintuna B, Lamari-Darkrim F, Hirscher M. Int. J. Hydrogen energy. Int J Hydrogen Energy 2007;32:1121.
[25] David WI. Effective hydrogen storage: a strategic chemistry challenge. Faraday Discuss 2011;151:399–414.
[26] Zaluski L, et al. Effects of relaxation on hydrogen absorption in Fe Ti produced by ball-milling. J Alloys Compd 1995;227(1):53–7.
[27] Erxleben A. Structures and properties of Zn (II) coordination polymers. Coord Chem Rev 2003;246(1–2):203–28.
[28] Kleperis J, et al. Zeolite as material for hydrogen storage in transport applications/CEOLĪTA KĀ ŪDEŅRAŽA UZGLABĀŠANAS VIDES IZPĒTE. Latv J Phys Tech Sci 2013;50(3):59–64.
[29] Xia Y, Yang Z, Zhu Y. Porous carbon-based materials for hydrogen storage: advancement and challenges. J Mater Chem A 2013;1(33):9365–81.
[30] Ozturk Z, et al. Hydrogen storage in heat welded random CNT network structures. Int J Hydrogen Energy 2015;40(1):403–11.
[31] Singh D, et al. High performance material for hydrogen storage: graphenelike Si2BN solid. Int J Hydrogen Energy 2017;42(36):22942–52.
[32] Er Sl, de Wijs GA, Brocks G. Hydrogen storage by polylithiated molecules and nanostructures. J Phys Chem C 2009;113(20):8997–9002.
[33] Tozzini V, Pellegrini V. Prospects for hydrogen storage in graphene. Phys Chem Chem Phys 2013;15(1):80–9.
[34] Wang L, Yang RT. New sorbents for hydrogen storage by hydrogen spillover–a review. Energy Environ Sci 2008;1(2):268–79.
[35] Kubas GJ. Metal–dihydrogen and σ-bond coordination: the consummate extension of the Dewar–Chatt–Duncanson model for metal–olefin π bonding. J Organomet Chem 2001;635(1–2):37–68.
[36] Rosi NL, et al. Hydrogen storage in microporous metal-organic frameworks. Science 2003;300(5622):1127–9.
[37] Cote AP, et al. Porous, crystalline, covalent organic frameworks. Science 2005;310(5751):1166–70.
[38] Felderhoff M, et al. Hydrogen storage: the remaining scientific and technological challenges. Phys Chem Chem Phys 2007;9(21):2643–53.
[39] Liang L, et al. Electronic bandgap and edge reconstruction in phosphorene materials. Nano Lett 2014;14(11):6400–6.
[40] Hu S, et al. Si 2 BN monolayers as promising candidates for hydrogen storage. Phys Chem Chem Phys 2020;22(24):13563–8.
[41] Huang X, et al. 25th Anniversary article: hybrid nanostructures based on two-dimensional nanomaterials. Adv Mater 2014;26(14):2185–204.
[42] Arellano J, et al. Density functional study of adsorption of molecular hydrogen on graphene layers. J Chem Phys 2000;112(18):8114–9.
[43] Li Q-F, et al. Theoretical prediction of hydrogen storage on Li-decorated monolayer black phosphorus. J Phys Appl Phys 2014;47(46):465302.
[44] Chen X, et al. Ca-decorated borophene as potential candidates for hydrogen storage: a first-principle study. Int J Hydrogen Energy 2017;42(31):20036–45.
[45] Varunaa R, Ravindran P. Potential hydrogen storage materials from metal decorated 2D-C 2 N: an ab initio study. Phys Chem Chem Phys 2019;21(45):25311–22.
[46] Yadav A, et al. Study of 2D MXene Cr2C material for hydrogen storage using density functional theory. Appl Surf Sci 2016;389:88–95.
[47] Shakil M, et al. Evaluation of hydrogen storage capacity of two-dimensional Sc2N MXene: a DFT study. Int J Hydrogen Energy 2024;69:740–8.
[48] Batool H, Majid A, Shahzadi I, Alkhedher M, Manan A, Haider S, Alam K. On the prospects of solid state hydrogen storage: first-principles investigations of two-Dimensional In2CO. Int J Hydrogen Energy 2024;95:510–9.
[49] Labrousse J, et al. High capacity hydrogen storage structure based on a two-dimensional material (Ga2C6) with strong adsorption properties. Int J Hydrogen Energy 2024;68:1072–9.
[50] Liu Z, Liu S, Er S. Hydrogen storage properties of Li-decorated B2S monolayers: a DFT study. Int J Hydrogen Energy 2019;44(31):16803–10.
[51] Zhong C, et al. Two-dimensional honeycomb borophene oxide: strong anisotropy and nodal loop transformation. Nanoscale 2019;11(5):2468–75.
[52] Naseri M, Hoat D. Prediction of a new 2D B2CO monolayer from density functional theory. Comput Mater Sci 2021;186:109975.
[53] Li F, et al. Two novel semiconducting B2CO monolayers with high carrier mobilities. J Comput Chem 2021;42(28):2024–30.
[54] Chen Y-T, Yeh C-H. Investigation of novel two-dimensional B2CO monolayer and its high sensing performance in detecting nitrogen-containing gases: a combined density functional theory calculation and non-equilibrium Green's function study. Sensor Actuator Phys 2024;369:115179.
[55] Orio M, Pantazis DA, Neese F. Density functional theory. Photosynth Res 2009;102:443–53.
[56] Cohen AJ, Mori-Sánchez P, Yang W. Challenges for density functional theory. Chem Rev 2012;112(1):289–320.
[57] Majid A., Zulfiqar R., Haider S., Alam K., Hassan, N. First principles study of structural and electronic properties of Ce substituted Ti_2O_3 slabs with compositions $Ti_xCe_{4-x}O_6$ where x = 0, 1, 2, 3, 4. Mater Sci Semicond Process 2024;180:108566.
[58] Perdew JP, Burke K, Ernzerhof M. Generalized gradient approximation made simple. Phys Rev Lett 1996;77(18):3865.
[59] Grimme S. Semiempirical GGA-type density functional constructed with a long-range dispersion correction. J Comput Chem 2006;27(15):1787–99.
[60] van Lenthe E, Baerends E-J, Snijders JG. Relativistic total energy using regular approximations. J Chem Phys 1994;101(11):9783–92.
[61] Batool H, Majid A, Alkhedher M, Bulut N, Al-Adwan IA. DFT study of quantum electronic transport properties of InTeCl. Mater Sci Semicond Process 2023;168:107842.
[62] Emery AA, Wolverton C. High-throughput DFT calculations of formation energy, stability and oxygen vacancy formation energy of ABO3 perovskites. Sci Data 2017;4(1):1–10.

[63] Hu S, et al. C7N6 monolayer as high capacity and reversible hydrogen storage media: a DFT study. Int J Hydrogen Energy 2021;46(42):21994–2003.
[64] Arab A, Habibzadeh M. Comparative hydrogen adsorption on the pure Al and mixed Al–Si nano clusters: a first principle DFT study. Comput. Theoret. Chem. 2015;1068:52–6.
[65] Singh M, Shukla A, Chakraborty B. Highly efficient hydrogen storage of a Sc decorated biphenylene monolayer near ambient temperature: ab initio simulations. Sustain Energy Fuels 2023;7(4):996–1010.
[66] Sun X, et al. Efficient hydrogen storage capacity of La3B18: a DFT study. Int J Hydrogen Energy 2023;48(21):7807–13.
[67] Sunandana C. Nanomaterials for hydrogen storage: the van't Hoff connection. Resonance 2007;12:31–6.
[68] Anikina E, et al. Li-decorated carbyne for hydrogen storage: charge induced polarization and van't Hoff hydrogen desorption temperature. Sustain Energy Fuels 2020;4(2):691–9.
[69] Li L, Zhang H, Cheng X. The high hydrogen storage capacities of Li-decorated borophene. Comput Mater Sci 2017;137:119–24.
[70] Mathew PT, Fang F. Periodic energy decomposition analysis for electronic transport studies as a tool for atomic scale device manufacturing. Int J Extrem Manuf 2020;2(1):015401.
[71] Jabeen A, Majid A, Alkhedher M, Haider S, Akhtar MS. Impacts of structural downscaling of inorganic molecular crystals-A DFT study of Sb2O3. Mater Sci Semicond Process 2023;166:107729.
[72] Shehbaz A, Majid A, Batool H, Alkhedher M, Haider S, Alam K. Probing the potential of Al 2 CO/SiC heterostructures for visible light-driven photocatalytic water splitting using first-principles strategies. J Mater Chem A 2024;12(21):12657–71.
[73] Chen K-H, et al. Efficient fast-charging of lithium-ion batteries enabled by laser-patterned three-dimensional graphite anode architectures. J Power Sources 2020;471:228475.
[74] Ahmed S, Alkhedher M, Isa M, Majid A. First principles study of layered CrGeTe3 as lithium intercalation compound. J Electrochem Soc 2022;169(4):040557.
[75] Henkelman G, Uberuaga BP, Jónsson H. A climbing image nudged elastic band method for finding saddle points and minimum energy paths. J Chem Phys 2000;113(22):9901–4.
[76] Majid A., Tasawar S., Raza H., Alam K., Alkhedher M., Haider S., Ahmed N. Uncovering the potential of two-dimensional SrRuO3 as anode material in Li, Na, Mg, Ca, K, and Zn ion batteries: first-principles investigations of structural, electronic and electrochemical properties. J Energy Storage 2025;105:114634.
[77] Wang Y, et al. Structure, reactivity, photoactivity and stability of Ti–O based materials: a theoretical comparison. Phys Chem Chem Phys 2012;14(7):2333–8.
[78] Silveri F, et al. Hydrogen adsorption on transition metal carbides: a DFT study. Phys Chem Chem Phys 2019;21(10):5335–43.
[79] Favot F, Dal Corso A. Phonon dispersions: performance of the generalized gradient approximation. Phys Rev B 1999;60(16):11427.
[80] Yang S, et al. A DFT study on the promising hydrogen storage performance of a light metal atom-decorated ZnO monolayer. Int J Hydrogen Energy 2024;50:71–83.
[81] Sha X, et al. Quantum studies of H atom trapping on a graphite surface. J Chem Phys 2005;122(1).
[82] Kerwin J, Sha X, Jackson B. Classical studies of H atom trapping on a graphite surface. J Phys Chem B 2006;110(38):18811–7.
[83] Li Y, Mi Y, Sun G. First principles DFT study of hydrogen storage on graphene with La decoration. J Mater Sci Chem Eng 2015;3(12):87.
[84] Huber K. Molecular spectra and molecular structure: IV. Constants of diatomic molecules. Springer Science & Business Media; 2013.
[85] Merlino AR, et al. A DFT study of hydrogen storage in Zr (Cr0. 5Ni0. 5) 2 Laves phase. Int J Hydrogen Energy 2016;41(4):2700–10.
[86] Kumar S, Samolia M, Dhilip Kumar TJ. Hydrogen storage in Sc and Li decorated metal–inorganic framework. ACS Appl Energy Mater 2018;1(3):1328–36.
[87] Faye O, et al. Hydrogen adsorption and storage on Palladium–functionalized graphene with NH-dopant: a first principles calculation. Appl Surf Sci 2017;392:362–74.
[88] Jain V, Kandasubramanian B. Functionalized graphene materials for hydrogen storage. J Mater Sci 2020;55(5):1865–903.
[89] Guo Y, et al. First-principles study of hydrogen storage on Ti-decorated B2C sheet. J Solid State Chem 2012;190:126–9.
[90] Li Y, Mi Y, Sun G. First principles DFT study of hydrogen storage on graphene with La decoration. J Mater Sci Chem Eng 2015;3(12):87–94.
[91] Chan KS, Miller MA, Peng X. First-principles computational study of hydrogen storage in silicon clathrates. Mater. Res. Lett. 2018;6(1):72–8.
[92] Bhatia SK, Myers AL. Optimum conditions for adsorptive storage. Langmuir 2006;22(4):1688–700.
[93] Schlapbach L, Züttel A. Hydrogen-storage materials for mobile applications. Nature 2001;414(6861):353–8.
[94] Zheng N, et al. A DFT study of the enhanced hydrogen storage performance of the Li-decorated graphene nanoribbons. Vacuum 2020;171:109011.
[95] Alhameedi K, et al. Metal functionalized inorganic nano-sheets as promising materials for clean energy storage. Appl Surf Sci 2019;471:887–92.
[96] Durgun E, Ciraci S, Yildirim T. Functionalization of carbon-based nanostructures with light transition-metal atoms for hydrogen storage. Phys Rev B 2008;77(8):085405.
[97] Yang X, et al. Two-dimensional aluminum phosphide semiconductor with tunable direct band gap for nanoelectric applications. RSC Adv 2020;10(42):25170–6.
[98] Azmat M, Majid A, Alkhedher M, Haider S, Akhtar MS. A first-principles study on two-dimensional tetragonal samarium nitride as a novel photocatalyst for hydrogen production. Int J Hydrogen Energy 2023;48(79):30732–40.
[99] Zhang Y, et al. A reversible hydrogen storage material of Li-decorated two-dimensional (2D) C4N monolayer: first principles calculations. Int J Hydrogen Energy 2021;46(65):32936–48.
[100] Zhang S, et al. Three-dimensional metallic boron nitride. J Am Chem Soc 2013;135(48):18216–21.
[101] Savin A, et al. ELF: the electron localization function. Angew Chem Int Ed Engl 1997;36(17):1808–32.
[102] Spencer MJ, Yarovsky I. ZnO nanostructures for gas sensing: interaction of NO2, NO, O, and N with the ZnO (1010) surface. J Phys Chem C 2010;114(24):10881–93.
[103] Sun Q, et al. First-principles study of hydrogen storage on Li12C60. J Am Chem Soc 2006;128(30):9741–5.
[104] Cui H, et al. Pd-doped MoS2 monolayer: a promising candidate for DGA in transformer oil based on DFT method. Appl Surf Sci 2019;470:1035–42.
[105] Cho S-Y, et al. Highly enhanced gas adsorption properties in vertically aligned MoS2 layers. ACS Nano 2015;9(9):9314–21.
[106] Lee H, et al. Calcium-decorated carbon nanotubes for high-capacity hydrogen storage: first-principles calculations. Phys Rev B 2009;80(11):115412.
[107] Li C, et al. High capacity hydrogen storage in Ca decorated graphyne: a first-principles study. J Phys Chem C 2011;115(46):23221–5.
[108] Du J, Jiang G. An aromatic Ca2B8 complex for reversible hydrogen storage. Int J Hydrogen Energy 2021;46(36):19023–30.
[109] Raupach M, Tonner R. A periodic energy decomposition analysis method for the investigation of chemical bonding in extended systems. J Chem Phys 2015;142(19).
[110] Hopffgarten Mv, Frenking G. Energy decomposition analysis. Wiley Interdiscip Rev Comput Mol Sci 2012;2(1):43–62.
[111] Raupach M, Tonner R. A periodic energy decomposition analysis method for the investigation of chemical bonding in extended systems. J Chem Phys 2015;142(19):194105.
[112] Mitoraj MP, Michalak A, Ziegler T. On the nature of the agostic bond between metal centers and β-hydrogen atoms in alkyl complexes. An analysis based on the extended transition state method and the natural orbitals for chemical valence scheme (ETS-NOCV). Organometallics 2009;28(13):3727–33.
[113] Pecher L, Tonner R. Deriving bonding concepts for molecules, surfaces, and solids with energy decomposition analysis for extended systems. Wiley Interdiscip Rev Comput Mol Sci 2019;9(4):e1401.
[114] Hu J, et al. A first-principles study of hydrogen storage of high entropy alloy TiZrVMoNb. Int J Hydrogen Energy 2021;46(40):21050–8.
[115] Yuan L, et al. First-principles investigation of hydrogen storage capacity of Y-decorated porous graphene. Appl Surf Sci 2017;399:463–8.
[116] Rahimi R, Solimannejad M. Empowering hydrogen storage performance of B4C3 monolayer through decoration with lithium: a DFT study. Surf Interfaces 2022;29:101723.
[117] Er S, de Wijs GA, Brocks G. Improved hydrogen storage in Ca-decorated boron heterofullerenes: a theoretical study. J Mater Chem A 2015;3(15):7710–4.
[118] Yang S, et al. A DFT study on the outstanding hydrogen storage performance of the Ti-decorated MoS2 monolayer. Surf Interfaces 2021;26:101329.
[119] Xie X, et al. First-principles studies in Mg-based hydrogen storage Materials: a review. Energy 2020;211:118959.
[120] Ströbel R, et al. Hydrogen storage by carbon materials. J Power Sources 2006;159(2):781–801.
[121] Liu H, et al. Y-decorated MoS2 monolayer for promising hydrogen storage: a DFT study. Int J Hydrogen Energy 2022;47(24):12096–106.
[122] Celik FA. Hydrogen adsorption and storage behaviors of Li-decorated PdS2 monolayer: an extended tight-binding study based on DFT. Int J Hydrogen Energy 2022;47(44):19146–54.
[123] Petrushenko I, Tsar'kova A, Petrushenko K. Hydrogen adsorption on BN-embedded tetrabenzopentacene as a promising nanoflake for energy storage: theoretical insights. Diam Relat Mater 2020;108:107968.
[124] Sathe RY. Ab-initio investigation of hydrogen sorption in Ti functionalized modified calix [4] pyrrole-benzene. Int J Hydrogen Energy 2020;45(51):27443–51.
[125] Konda R, et al. Functionalized tetrahedral silsesquioxane cages for hydrogen storage. Int J Hydrogen Energy 2020;45(56):32157–67.
[126] Tarasov BP, et al. Metal hydride hydrogen storage and compression systems for energy storage technologies. Int J Hydrogen Energy 2021;46(25):13647–57.
[127] Keow ALJ, et al. Active disturbance rejection control of metal hydride hydrogen storage. Int J Hydrogen Energy 2021;46(1):837–51.
[128] Guo C, Wang C. The effect of charge on the dihydrogen storage capacity of Sc2–C6H6. Int J Hydrogen Energy 2021;46(1):955–66.
[129] Koizumi K, Nobusada K, Boero M. Hydrogen storage mechanism and diffusion in metal–organic frameworks. Phys Chem Chem Phys 2019;21(15):7756–64.
[130] Prasetyo N, Pambudi FI. Toward hydrogen storage material in fluorinated zirconium metal-organic framework (MOF-801): a periodic density functional theory (DFT) study of fluorination and adsorption. Int J Hydrogen Energy 2021;46(5):4222–8.
[131] Wen T, et al. Novel Ti-decorated borophene χ3 as potential high-performance for hydrogen storage medium. Int J Hydrogen Energy 2020;45(53):29059–69.
[132] Dillon AC, et al. Storage of hydrogen in single-walled carbon nanotubes. Nature 1997;386(6623):377–9.
[133] Dillon AC, et al. Carbon nanotube materials for hydrogen storage. Proc. 2000 DOE/NREL Hydrogen program review 2000:8–10.

[134] Züttel A. Hydrogen storage methods. Naturwissenschaften 2004;91:157–72.
[135] Schlapbach L, et al. Hydrogen for novel materials and devices. Appl Phys A 2001; 72:245–53.
[136] Lee H-S, Vermaas WF, Rittmann BE. Biological hydrogen production: prospects and challenges. Trends Biotechnol 2010;28(5):262–71.
[137] Xu W-C, et al. Investigation of hydrogen storage capacity of various carbon materials. Int J Hydrogen Energy 2007;32(13):2504–12.
[138] Lee SM, Lee YH. Hydrogen storage in single-walled carbon nanotubes. Appl Phys Lett 2000;76(20):2877–9.
[139] Han SS, Lee HM. Adsorption properties of hydrogen on (10, 0) single-walled carbon nanotube through density functional theory. Carbon 2004;42(11): 2169–77.
[140] Züttel A. Materials for hydrogen storage. Mater Today 2003;6(9):24–33.
[141] Pinkerton FE, et al. Thermogravimetric measurement of hydrogen absorption in alkali-modified carbon materials. J Phys Chem B 2000;104(40):9460–7.